doi:10.26443/seismica.v3i2.1384

# Putting faults in the northern Chilean subduction margin into motion: evidence for remote dynamic earthquake triggering near the plate interface and within the forearc

**Rebecca M. Harrington** * [1], **Debi Kilb** [2], **Marco P. Roth** [1], **Pia Victor** [3], **Alessandro Verdecchia** [1]

[1]Institute for Geology, Mineralogy and Geophysics, Ruhr University Bochum, Germany, [2]Scripps Institution of Oceanography, University of California, San Diego, La Jolla, California, 92093-0225 USA, [3]Helmholtz Centre Potsdam, GFZ German Research Centre for Geosciences, Germany

Author contributions: *Conceptualization*: R. M. Harrington. *Methodology*: R. M. Harrington, D. Kilb. *Software*: R. M. Harrington, D. Kilb, M. P. Roth. *Formal Analysis*: R. M. Harrington, D. Kilb, A. Verdecchia, M. P. Roth. *Investigation*: R. M. Harrington, D. Kilb, P. Victor. *Writing - Original draft*: R. M. Harrington, D. Kilb. *Writing - Review & Editing*: R. M. Harrington, D. Kilb, P. Victor, M. P. Roth. *Visualization*: R. M. Harrington, D. Kilb. *Supervision*: R. M. Harrington. *Project administration*: R. M. Harrington.

**Abstract** Dynamic stresses on the order of ∼1 kPa from passing waves of mainshock earthquakes can trigger aftershocks at remote distances. Here, we investigate the prevalence of remote earthquake triggering in northern Chile, where aseismic-slip triggering has been documented. Our twofold approach to quantify triggerability includes a statistical difference-of-means test to quantify seismicity-rate changes bracketing candidate mainshock times, and a waveform-based approach to look for triggered earthquakes missing from the local catalog. We find no persistent, statistically-significant seismicity-rate increases associated with any of the candidate mainshocks when considering the local catalog in aggregate. However, catalog statistics reveal evidence for localized triggering both near the subduction interface and within the shallower forearc faults. Waveforms reveal local, uncataloged earthquakes visible only after applying a high-pass filter that removes the mainshock signal that otherwise overprints and obscures these local signals. Based on Japan mainshocks, we cannot rule out antipodal triggering. Areas showing higher triggerability are consistent with regions of low locking inferred from GNSS models and regions of observed aseismic slip. The spatial coincidence of triggering and low-locking, combined with the absence of a stress-triggering threshold, requires non-linear triggering mechanisms, such as altered frictional strength or aseismic-slip triggering, to be consistent with the observations.

Production Editor: Gareth Funning
Handling Editor: Andrea Llenos
Copy & Layout Editor: Kirsty Bayliss

Signed reviewer(s): Bogdan Enescu

Received: June 5, 2024
Accepted: September 30, 2024
Published: November 6, 2024

**Non-technical summary** It has been known for decades that large earthquakes can trigger distant aftershocks, a phenomenon called "remote aftershock triggering". The physics of remote triggering is not fully understood, as it only occurs in some regions. However, remote triggering is likely caused by transient shaking from passing seismic waves that generate primarily temporary changes. Here, we explore the capability of a suite of 29 large (magnitude 6.8+) earthquakes to trigger remote aftershocks (distances of 500+ km) within the northern Chilean subduction margin. Applying statistical measurements to a local earthquake catalog shows localized regions where triggering is more prevalent. Examining seismic waveforms reveals additional remote triggering from earthquakes not included in the catalog. The reason that waveforms reveal more instances of triggering is that many local earthquakes are only visible after applying a high-pass filter that removes the mainshock signal that otherwise masks these local signals. We find no stress amplitude threshold required for remote triggering, suggesting multiple processes might be working in tandem. The areas which exhibit increased triggering capability are near regions where fault properties vary, and may help explain the mechanisms by which earthquakes start.

## 1 Introduction

Earthquakes interact with one another over a range of distances. The static-stress changes, which result from the permanent offset on a fault after an earthquake occurs, decay rapidly with distance (proportional to $1/r^3$, where $r$ is distance) and become negligible at distances greater than ∼1-2 fault lengths (Stein, 1999; Prejean et al., 2004; Freed, 2005; Prejean and Hill, 2018). Static-stress changes can promote or inhibit failure on neighboring (so-called receiver) faults depending on whether they invoke a positive or negative shear stress change, and earthquakes generated as a direct result of static-stress changes are typically termed "aftershocks" (e.g., Stein, 1999). Earthquakes also generate transient stress changes imparted by the ground motion of their passing seismic waves at greater distances than static-stress changes. The transient "dynamic" stress changes, imparted to receiver faults by dynamic shaking, decay

*Corresponding author: rebecca.harrington@rub.de

more slowly in space relative to static-stresses ($1/r^2$), and are assumed to collectively impart primarily positive stress changes, which can only promote aftershocks, not inhibit them. Aftershocks that are triggered by dynamic-stress changes are termed "remotely triggered" and have been observed at distances of up to ~20 fault lengths or more, both immediately following the passage of the mainshock waves and with delays of many hours or days (Hill et al., 1993; King et al., 1994; Kilb et al., 2000; Gomberg et al., 2001; Miyazawa, 2011; Brodsky and van der Elst, 2014; Aiken and Peng, 2014; Opris et al., 2018; Prejean and Hill, 2018). Recent studies suggest that static and dynamic triggering can both occur in the near field, contributing 2/3 and 1/3 of the triggering capabilities, respectively (e.g., Hardebeck and Harris, 2022).

When remote aftershock triggering occurs on immediate time scales, it typically does so during the passage of the larger amplitude surface waves, and the triggered events are commonly small in magnitude ($M<2$) (e.g., Hill et al., 1993; Gomberg et al., 2001; Husen et al., 2004; Hernandez et al., 2014). Both immediately and delayed triggered events are common near geothermal regions (e.g., Enescu et al., 2016). However, the perceived ubiquity of triggering in geothermal regions may be correlated with the heightened historical detection capability of seismic networks in such regions (Prejean and Hill, 2018). More recent work suggests that triggering propensity might be generally ubiquitous and made up of primarily small-magnitude events (e.g., Fan et al., 2021), albeit locally heterogeneous (e.g., Pankow and Kilb, 2020).

Remote dynamic triggering of larger ($M>5$) earthquakes has also been documented (e.g., Johnson et al., 2015). Yet, exploring the causality, timing, and possible triggering mechanisms of the more common and numerous small-magnitude triggered earthquakes is facilitated by the differences in frequency content of the causative triggering mainshock and triggered aftershocks. For example, when observed, immediate triggering commonly occurs during the passage of surface waves (Pankow et al., 2004; Prejean et al., 2004; Brodsky and Prejean, 2005; Velasco et al., 2008; Aiken and Peng, 2014). Converting surface wave ground motions to stress values offers the opportunity to quantify the magnitude of the stress perturbation that leads to earthquake nucleation. Many studies document immediate triggering caused by stress values estimated to be on the order of tidal stresses (~1-10 kPa or more), suggesting that the faults on which triggered earthquakes occur are critically stressed and/or possibly at the end of their seismic cycle (Brodsky and Prejean, 2005; Aiken and Peng, 2014; Wang et al., 2018).

The process(es) by which stress perturbations of ~1 kPa can result in both immediate and delayed remote aftershock triggering has made identifying a causative mechanism(s) that can explain the range of observations challenging. The Coulomb Failure Stress model has been successfully invoked where observations allow constraining receiver fault geometry (e.g., Tape et al., 2013). But there are many documented cases that demonstrate how threshold-type behavior (for which a given stress transient generates a change in earthquake rate) is often inconsistent with observations (e.g., Gomberg et al., 2001; Bansal and Ghods, 2021). Brodsky and Prejean (2005) noted that threshold-like behavior may be present when considering frequency content. Other studies have documented examples showing a weaker dependence of triggerability on frequency, suggesting that, at least in some faulting environments, it may play a secondary role (Fan et al., 2021). Much work has explored other factors that may influence triggerability, such as tectonic environment, mainshock back-azimuth, directivity of seismic energy, and the focal mechanism of the triggering mainshock (Gomberg et al., 2004; Hill, 2015; Alfaro-Diaz et al., 2020; Fan et al., 2021; Dixit et al., 2023). But, no single factor has proven to universally explain the variability in observations, suggesting that multiple mechanisms may be responsible for nucleating triggered earthquakes.

Linear, threshold-type triggering mechanisms suggest that triggering may be easier in transtensional or extensional faulting environments (Hill, 2015). Yet, non-linear responses to small stress perturbations and delayed triggering effects suggest that additional mechanisms may be at work, such as temporal or spatial variability of frictional properties, material fatigue, aseismic slip triggering, or secondary cascading effects, such as pore-pressure redistribution (Wei et al., 2015; Johnson et al., 2016; Jin et al., 2021; Yu et al., 2021). In particular, aseismic slip serves as a viable mechanism to potentially explain both immediate and delayed triggering. While harder to observe, there are documented cases of aseismic slip triggering, either inferred by the progression of nearby associated low-frequency seismic signals (e.g., Shelly et al., 2011; Gombert and Hawthorne, 2023), or inferred directly by observations (e.g., Guglielmi et al., 2015; Wei et al., 2015; Wallace et al., 2017). In particular, Victor et al. (2018) documented examples of remote aseismic slip triggering within the subduction forearc in northern Chile caused by passing surface waves of remote mainshocks. The authors used colocated creepmeter and seismometer data to infer a causal relationship between the mainshock surface-wave shaking and the resultant aseismic slip.

Here, we quantify the triggering propensity of seismic events in the same study region of Victor et al. (2018) at two spatial resolutions, one large scale (100s of km), including the full study region, and one small scale, within circular sub-regions of ~20 km radius. We first use the coarser length scale to examine the broad triggering propensity (or triggerability) on a regional scale to establish if triggering is common. We then quantify triggerability at higher resolution to establish the heterogeneity of triggering behavior and any possible correlation with geological or faulting conditions. We use a newly published local earthquake catalog from Sippl et al. (2023) and waveform data from the Chilean National Seismic Network stations, and focus on the shallow forearc faults of the Atacama fault system as well as the plate interface zone and neighboring faults in the subduction system. In our investigation, we use a twofold approach, using catalog statisti-

cal tests and waveform signal behavior to quantify the triggerability of the study region to stress changes from 29 remote mainshocks. Our aim is to provide a broad-scale regional study of triggering in northern Chile and identify local areas of high triggering potential. Our observations will ultimately allow us to pinpoint viable triggering mechanisms, and rule out mechanisms that are inconsistent with our findings. Using our candidate mainshock selection criteria, statistical methods, and waveform investigation, we find that triggerability is elevated in regions where fault locking may be low relative to surrounding regions, and that non-linear mechanisms are needed to explain these observations.

## 2 Data and Methods

The search for remote triggering in northern Chile is based on an approach that explores two end-member search methods. The first method quantifies statistical changes in local seismicity rates within relatively long time windows bracketing seismic wave arrivals from remote mainshocks ($\pm$1 to $\pm$14 days). The second focuses on the elevated signals within 3-component waveform data spanning relatively short time windows (one hour before the initial seismic wave arrival until one hour after the last seismic wave passage). The former (catalog-based) and latter (waveform-based) approaches use different data types.

The catalog-based method quantifies changes in local seismicity bracketing stressing events (i.e., candidate mainshocks) using a new, local seismicity catalog described in Sippl et al. (2023). The Sippl et al. (2023) catalog is an expansion of previous work (Sippl et al., 2018) that includes an additional seven years of data and phase picks from a larger number of stations. This new 2023 catalog includes data from 2007-2021. Catalog building uses a semi-automated approach for phase identification for use in computing nearly 183,000 relocated hypocenters with <5 km uncertainty inside the footprint of the network. The overall magnitude of completeness is estimated at M2.7 (Hainzl et al., 2019).

We quantify rate changes in the local earthquake catalog surrounding each stressing event caused by the passing waves of remote candidate mainshocks. A significant number of earthquakes within the study area generated large stress transients ($\geq$ 10 kPa) that occurred during the catalog period, including the sequence related to the 1 April 2014 M8.2 Iquique mainshock. Because triggering in the near-field may result from either static- and/or dynamic-stress (strain) changes (e.g., van der Elst and Brodsky, 2010; Hardebeck and Harris, 2022), we restrict our candidate mainshocks to only remote events (distances 500 km or more), where static triggering stresses are negligible.

The waveform-based method estimates if earthquakes are missing from the local catalog by analyzing high-pass filtered waveforms recorded at local stations. The long-period large-amplitude surface waves from candidate mainshocks can dwarf smaller, local earthquake signals. When the passing teleseismic surface waves mask local signals, it can be problematic for routine catalog-building efforts, as the hidden local events may not be counted (e.g., Brodsky and Prejean, 2005). However, remote and local earthquakes have different frequency contents, where local events have more energy concentrated in higher-frequency bands above ~5Hz than remote events. Applying a 5 Hz high-pass filter to teleseismic waveforms allows local earthquake signals to become more visible within the wavetrains. We examine filtered waveforms recorded across the CX, 8G, and 8F local networks within our study region (Fig 1) in $\pm$ 1-hour time windows bracketing the seismic waves from each candidate mainshock. The goal is not to catalog each small event but instead to intuit if there is an increase in the seismic wave amplitudes within these time windows indicative of local rate increases, suggesting a higher rate change than reported from the local catalog rate change values.

Our analysis approach includes three primary steps: (1) selecting candidate mainshocks, (2) identifying elevated triggering activity using local catalog statistics, and (3) exploring characteristics of 3-component waveform data recorded at local seismic stations. We detail each of these three tasks in the following subsections.

### 2.1 Candidate mainshock selection based on peak-ground-velocity (PGV) estimates

Although past work has consistently emphasized that large peak dynamic-stress, or large ground motions, are not likely the sole trigger of remote aftershocks (Kane et al., 2007; Fan et al., 2021), it remains likely that large amplitudes do play some role in remote triggering processes, particularly when considering long-period shaking (Brodsky and Prejean, 2005; Prejean et al., 2010; van der Elst and Brodsky, 2010; Fan et al., 2021). Therefore, to begin, we identify mainshocks that theoretically produce large dynamic-stresses at our study region's centroid (-22°N, -70°E). We use the catalog magnitude to estimate a peak amplitude (Eq. 1), with which we assign a theoretical peak ground velocity (PGV) and corresponding dynamic-stress value to each of the 11,878 mainshocks that occurred during the time period of our local catalog from 1 January 2007 - 31 December 2021 (Eqs. 2 and 3). The theoretical peak stress amplitudes allow for a comparison with those that produced known remote triggering of aseismic slip events (i.e., the M8.8 Maule earthquake and the M9.0 Tohoku earthquake (Victor et al., 2018)).

Our theoretical dynamic strain and peak ground velocity (PGV) estimates are computed following the method of Lay and Wallace (1995). Far-field dynamic strain can be estimated as in van der Elst and Brodsky (2010):

$$\log A_{20} = M_s - 1.66 \log \Delta - 2 \quad (1)$$

Where $A_{20}$ is peak surface wave amplitude (in $\mu$m) for 20-second period surface waves, $M_s$ is surface wave magnitude, and $\Delta$ is the epicentral distance in degrees. We assign $M_s$ to the ANSS Comprehensive Earthquake Catalog (ComCat) (U. S. Geological Survey, 2024) magnitude in Eq. 1, which we realize might be in error for shallow events, but should provide a sufficient guideline.

PGV is approximated by Aki and Richards (2002); van der Elst and Brodsky (2010):

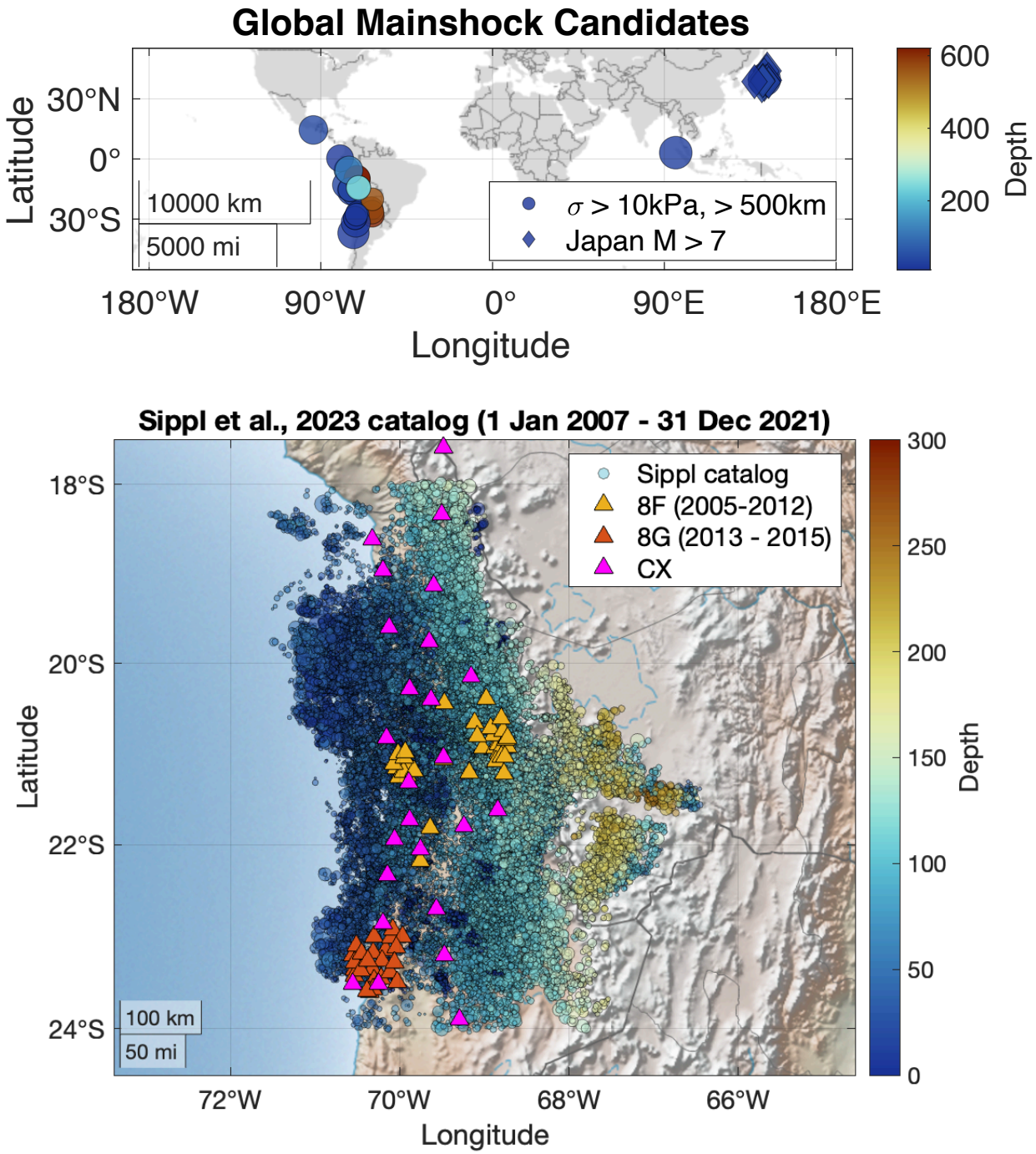


**Figure 1** Candidate triggering mainshocks and study area in Northern Chile. (a) Global mainshocks at distances > 500 km from the center of the study area (circles) that generated stresses >10 kPa and events in Japan with $M$>7 that occurred at epicentral distances within 500 km of the 2011 $M9.1$ Tohoku-Oki, Japan, earthquake (diamonds). (b) Seismicity from the Sippl et al. (2023) catalog (dots; N=182,841; color-coded by depth) and 3-component seismic stations (triangles color-coded by network: CX (pink) corresponds to the permanent IPOC network stations, Feb 2006 - present; Temporary networks 8F (orange), Oct 2005 - March 2012; 8G (red), June 2013 - October 2015). Networks 8F and 8G were operated by the FU Berlin and Geoforschungszentrum Potsdam (see Data section for details).

$$PGV \approx 2\pi * A_{20}/T \tag{2}$$

And, in turn, dynamic-stress change becomes:

$$\sigma = \mu * PGV/V_{ph} \tag{3}$$

Where $\mu$ is the shear modulus, assumed to be 35GPa, and $V_{ph}$ is the surface wave velocity assigned to 3.5 km/s (Li et al., 2023). While the elastic material properties are expected to vary greatly over the depth range of local seismicity, the approximations for shear modulus and surface wave velocity are only meant to provide a reasonable value to cull the candidate list of mainshocks.

We use a threshold cutoff of 8 kPa for the peak dynamic mainshock stress to quantify the triggering potential of the candidate mainshocks. The cutoff is cho-

sen to lie safely below the value of ∼10 kPa for which triggering has been clearly established in a number of other regions (e.g., Brodsky and Prejean, 2005; Aiken and Peng, 2014; Wang et al., 2018). Imposing this 8 kPa cutoff on the initial ComCat dataset leaves 18 M6.8+ global earthquakes at distances ≥ 500 km from the centroid of our study region that occurred between 2007 through 2021 (0.15% of the original data set).

We augment our base catalog of 18 global candidate mainshocks with a secondary catalog of 11 large earthquakes (M7+) from Japan, located within 500 km from the largest 2011 M9.1 Tohoku earthquake. The motivation for including these Japanese events is twofold. First, the 2011 M9.1 Japan earthquake produced measurable strain changes on creep meters in the Atacama Fault System that triggered shallow aseismic slip transients (Victor et al., 2018). Second, because these Japan earthquakes are 145°-152° arc length from the centroid of our study region, or equivalently, within approximately 30° from the mainshock antipodes. Previous work has suggested that aftershock triggering may be more likely to occur near the mainshock antipode because the larger amplitude surface waves might constructively combine to produce elevated ground motions (O'Malley et al., 2018). Including the 11 additional Japanese earthquakes allows us to test for repeat triggering of seismic slip for similar distance/azimuth pairs. Table 1 provides a list of the candidate mainshocks that meet the criteria detailed above, including origin information, distance from the study area, and estimated peak dynamic-stress values.

## 2.2 Statistical methods used to identify seismicity-rate changes

Observations in which a stress perturbation from passing seismic waves can be unambiguously linked to a subsequent (i.e., triggered) local earthquake on time scales of minutes or hours are comparatively rare (e.g., Gomberg et al., 2001; Prejean et al., 2004; Aiken and Peng, 2014). Such immediate triggering has been documented to occur in what appear to be favorable conditions, such as geothermal settings with high seismicity rates, often in trans-tensional or extensional tectonic regimes. Observing immediate triggering commonly requires more in-depth waveform analysis (e.g., Brodsky and Prejean, 2005; Prejean and Hill, 2018). Nevertheless, much work has documented observable seismicity-rate changes found within seismic catalogs over local, regional, and global scales following stress perturbations imparted by the passing waves of remote earthquakes (Gomberg et al., 2001; Pollitz et al., 2012; Prejean and Hill, 2018; DeSalvio and Fan, 2023). A commonly accepted approach to test for the likelihood of triggering uses some form of a statistical difference-of-means test to quantify whether a null hypothesis of no observed seismicity-rate changes can be rejected according to a specified confidence level.

We adopt a similar approach to Wang et al. (2019) that quantifies the probability of a change in the average seismicity rate before and after a stressing event, respectively, $\lambda_b$ and $\lambda_a$. Here, subscripts $b$ and $a$ refer to "before" and "after" the stressing event, and the stressing event refers to the mainshock origin time. The theoretical upper limit of stress perturbation is described by Eq. 3 in Section 2.1. We assume the magnitude of stress perturbation inferred from Eq. 3 represents an upper limit, because we do not know the orientation of the receiver fault in relation to the incoming seismic waves. Only in cases where receiver-fault orientations are known can the resolved shear stress be more precisely computed (Tape et al., 2013). The statistical test employed here follows a common assumption in triggering studies, namely, that the background seismicity is well-described by a Poisson distribution and that possible triggered sequences exhibit a time decay governed by Omori's Law (Reasenberg, 1985; Ogata, 1999; Brodsky and van der Elst, 2014). If we consider the number of earthquakes, $n$, that occur in a given time window, $t$, then $\lambda = n/t$ describes the average earthquake occurrence rate. Based on the assumption of a Poisson process, the following equation then describes the probability, $P$, of observing $n$ earthquakes in time period $t$, given an average rate $\lambda$:

$$P_n(N_{eq} = n|\lambda t) = \frac{(\lambda t)^n e^{-\lambda t}}{n!} \tag{4}$$

Dynamic triggering corresponds to a step-wise increase in a Poisson process, meaning that the background rate after the stressing event, $\lambda_a$, will change in the presence of triggering. If we consider time periods of equal duration before and after the stressing event, such that $t_b = t_a$, we can quantify the probability of a rate change relative to $\lambda_b$ (the average rate prior to the mainshock) using the number of earthquakes that occurred after the stressing event, $n_a$, and the cumulative probability distribution of $P_n$ (Eq. 4). The probability $P$ of observing $n_a$ events in a time window $t_b = t_a$ is then given by the following equation,

$$P(n_a|\lambda_b t_b) = e^{-\lambda_b t_b} \sum_{i=0}^{n_a} \frac{(\lambda_b t_b)^i}{i!} \tag{5}$$

In this work, our null hypothesis is that no significant seismicity rate changes occur following the stressing event, i.e. that $\lambda_b \approx \lambda_a$.

$P$ in Eq. 5 indicates the probability with which the null hypothesis can be rejected. Thus, $P \geq 0.95$ indicates that the null hypothesis (no seismicity increase) can be rejected, and the result is robust at a statistical significance corresponding to 95% (or $2\sigma$). $P$-values below 0.5 would suggest a seismicity-rate decrease occurred after the stressing event. Here, we assume that any rate decreases inferred from low $P$-values are the result of other processes (e.g. natural rate fluctuations or stress decreases from other mechanisms), given that dynamic-stress changes are exclusively associated with positive rate changes (e.g., Kilb et al., 2000; Meng and Peng, 2014).

Past work has established that dynamic triggering can occur both immediately during the passage of surface waves, as well as over delayed time scales ranging from days to weeks (e.g., Gomberg et al., 2001; Peña Castro et al., 2019). We therefore calculate $P$-values for a range

of time windows that span up to two weeks before and after a candidate mainshock, namely $t = t_b = t_a = 1$, 7, 10, and 14 days. The range of time windows allows us to compare $P$-values of variable duration and more easily flag anomalous behavior. It also allows us to assess if triggering in this region tends to occur more in the short-term or long-term (Prejean and Hill, 2018).

Initially, we use the entire local catalog and Eq. 5 to calculate $P$-values (one for each of the four time windows noted above) for each of the global candidate mainshocks in Tab. 1. In addition to calculating $P$-values for all events in aggregate, we also look at the $P$-value distribution of events with hypocentral locations above and below depths of 60 km. The 60 km depth distinction provides a first-order separation of shallower seismicity in the forearc from the deeper seismicity on the plate interface, the slab, and the mantle wedge. This 60 km depth distinction follows the event-type classification outlined by Sippl et al. (2023).

Several studies have found evidence for localized instances of triggering, suggesting that a broad, regional search may risk dwarfing possible triggering signals, especially in regions of high seismicity rates (Wang et al., 2015; Pankow and Kilb, 2020; DeSalvio and Fan, 2023), such as those in northern Chile. We, therefore, also calculate $P$-values for smaller, circular, overlapping regions using the same time windows (±1, 7, 10, and 14 day intervals) for each of the 29 candidate mainshocks (Tab. 1) to explore if rate changes occur in localized regions. These circular sub-regions are centered on grid nodes placed at 0.2° intervals within the study area and have radii of 0.2° (∼20 km) encompassing each node. The 0.2° node spacing and ∼20 km radial extent ensure the circles overlap and there are no gaps (see Fig. S1 for a graphic of the node spacing and overlapping circular areas).

To avoid statistics of small numbers, we require at least $n_a \geq 10$ and $n_b \geq 10$ events to merit a $P$-value calculation for a given node when computing $P$-values within the smaller spatial grids. Additionally, we select only events that produce grid nodes in which the $P$-value exceeds 0.95 for at least one of the first three time windows (i.e., ±1, 7, or 10 days). For nodes that pass these two criteria, the average $P$-value for all candidate mainshocks for a given time-window length are computed and assigned to that node. We then assess the triggerability by selecting the maximum, mainshock-averaged $P$-value for an individual node over the range of time windows considered (±1, 7, 10, and 14 days). This gridded P-value calculation allows us to identify anomalous triggering behavior over a more refined spatial scale.

Natural seismicity fluctuations could cause statistically significant rate changes at individual nodes by random chance. Should random increases be present, they would likely exhibit a lack of spatial correlation, making it more difficult to confidently attribute random grid nodes with elevated $P$-values to triggering. We therefore also test the susceptibility of our approach to measure high triggerability by chance by using data from 20 random origin times not associated with large earthquakes. We select random time windows, although we specifically avoid data from the two months following the 01 April 2014 M8.2 Iquique mainshock sequence, when the local seismicity rates were clearly disrupted. We repeat the same statistical analysis outlined above to process the random time-windows and calculate the maximum, mainshock-averaged $P$-value for each grid node (i.e., the measure of triggerability). The grid node $P$-values for the true events can then be compared with the random results.

## 2.3 Identification of elevated waveform amplitudes caused by local earthquakes

Statistical tests that reveal significant seismicity-rate increases associated with specific mainshocks offer compelling circumstantial evidence of triggering. Yet, if small-magnitude ($M<2$) earthquakes are missing from the catalogs, these statistical tests might be misleading. We therefore augment the statistical tests with waveform analysis. We focus on stations near sites where Victor et al. (2018) documented aseismic slip triggering, and where gridded $P$-value estimates suggest localized areas of higher triggerability (shown in Section 3.1).

We explore the possibility that triggered earthquakes dwarfed by mainshock shaking are missing from the local catalog using the following method. First, for stations of interest, we collect 3-component waveform data spanning ±1 hour prior to and after the first and last theoretical seismic wave arrivals, respectively. The first and last phase arrivals for all but one of the candidate distant earthquakes are $P_{diff}$ and SKIKSSKIKS phases. The only exception to this is the 04 April 2018 event, which theoretically has the P-wave as the first seismic wave arrival. After removing the mean from each waveform, we apply a 5 Hz highpass 4th order Butterworth filter. The highpass filter removes the lower frequency signals from the teleseismic events, while maintaining the higher-frequency local signals.

To gain a general sense of when elevated signals occur, we use a simple binary approach to indicate what time steps have elevated signals. Importantly, we do not aim to identify each individual earthquake. The goal is to obtain a general understanding of the cumulative duration of elevated signals within a given time period during the teleseismic wave passage, and better estimate how many potentially triggered smaller earthquakes are missing from the local catalog. From the envelope of each waveform, we compute the mean and standard deviation and flag times when the envelope signal exceeds the mean plus two standard deviations. We only compute envelopes for recordings with all three components of data; data lacking three components are ignored. These binary measurements (elevated or not elevated) are made for each time step where time zero is assigned to the time of the first teleseismic wave arrival.

For each waveform, we track the cumulative number of elevated measurements as a function of time. As a final step, we stack all the values from all stations and all channels. These cumulative measurements can also help flag noisy data, as the signature of the elevated signals in the noisy data looks very different than the signature from the other stations. This makes it easy to iden-

| Index | Year | Month | Day | Hour | Min | Sec | Lat. (°N) | Lon. (°E) | Depth (km) | Magnitude | Distance (km) | Stress (kPa) |
|---|---|---|---|---|---|---|---|---|---|---|---|---|
| 1 | 2007 | 8 | 15 | 23 | 40 | 57.0 | -13.4 | -76.6 | 39 | 8.0 | 1185 | 62 |
| 2 | 2010 | 2 | 27 | 6 | 34 | 11.0 | -36.1 | -72.9 | 23 | 8.8 | 1595 | 238 |
| 3 | 2011 | 1 | 1 | 9 | 56 | 58.0 | -26.8 | -63.1 | 577 | 7.0 | 876 | 10 |
| 4 | 2011 | 3 | 11 | 5 | 46 | 24.0 | 38.3 | 142.4 | 29 | 9.1 | 16439 | 10 |
| 5 | 2013 | 1 | 30 | 20 | 15 | 43.0 | -28.1 | -70.7 | 45 | 6.8 | 680 | 10 |
| 6 | 2013 | 9 | 25 | 16 | 42 | 43.0 | -15.8 | -74.5 | 40 | 7.1 | 833 | 14 |
| 7 | 2015 | 9 | 16 | 22 | 54 | 32.0 | -31.6 | -71.7 | 22 | 8.3 | 1077 | 145 |
| 8 | 2015 | 11 | 11 | 1 | 54 | 38.0 | -29.5 | -72.0 | 12 | 6.9 | 859 | 8 |
| 9 | 2015 | 11 | 11 | 2 | 46 | 19.0 | -29.5 | -72.1 | 10 | 6.9 | 860 | 8 |
| 10 | 2015 | 11 | 24 | 22 | 45 | 38.0 | -10.5 | -70.9 | 606 | 7.6 | 1278 | 22 |
| 11 | 2015 | 11 | 24 | 22 | 50 | 54.0 | -10.1 | -71.0 | 621 | 7.6 | 1332 | 20 |
| 12 | 2016 | 4 | 16 | 23 | 58 | 36.0 | 0.4 | -79.9 | 21 | 7.8 | 2711 | 10 |
| 13 | 2017 | 9 | 8 | 4 | 49 | 19.0 | 15.0 | -93.9 | 47 | 8.2 | 4871 | 9 |
| 14 | 2018 | 1 | 14 | 9 | 18 | 45.0 | -15.8 | -74.7 | 39 | 7.1 | 852 | 13 |
| 15 | 2018 | 4 | 2 | 13 | 40 | 34.0 | -20.7 | -63.0 | 559 | 6.8 | 739 | 9 |
| 16 | 2019 | 3 | 1 | 8 | 50 | 42.0 | -14.7 | -70.2 | 267 | 7.0 | 811 | 12 |
| 17 | 2019 | 5 | 26 | 7 | 41 | 15.0 | -5.8 | -75.3 | 123 | 8.0 | 1887 | 29 |
| 18 | 2020 | 9 | 1 | 4 | 9 | 28.0 | -28.0 | -71.3 | 21 | 6.8 | 677 | 10 |
| 1 | 2008 | 7 | 19 | 2 | 39 | 28.7 | 37.6 | 142.2 | 22 | 7.0 | 16483 | 0.1 |
| 2 | 2011 | 3 | 9 | 2 | 45 | 20.3 | 38.4 | 142.8 | 32 | 7.3 | 16397 | 0.2 |
| 3 | 2011 | 3 | 11 | 5 | 46 | 24.1 | 38.3 | 142.4 | 29 | 9.1 | 16441 | 9.9 |
| 4 | 2011 | 3 | 11 | 6 | 15 | 40.3 | 36.3 | 141.1 | 43 | 7.9 | 16623 | 0.6 |
| 5 | 2011 | 3 | 11 | 6 | 25 | 50.3 | 38.1 | 144.6 | 19 | 7.7 | 16268 | 0.4 |
| 6 | 2011 | 4 | 7 | 14 | 32 | 43.3 | 38.3 | 141.6 | 42 | 7.1 | 16506 | 0.1 |
| 7 | 2011 | 7 | 10 | 0 | 57 | 10.8 | 38.0 | 143.3 | 23 | 7.0 | 16378 | 0.1 |
| 8 | 2012 | 12 | 7 | 8 | 18 | 23.1 | 37.9 | 143.9 | 31 | 7.3 | 16327 | 0.2 |
| 9 | 2013 | 10 | 25 | 17 | 10 | 19.7 | 37.2 | 144.7 | 35 | 7.1 | 16292 | 0.1 |
| 10 | 2021 | 2 | 13 | 14 | 7 | 49.8 | 37.7 | 141.8 | 44 | 7.1 | 16513 | 0.1 |
| 11 | 2021 | 3 | 20 | 9 | 9 | 44.0 | 38.5 | 141.6 | 43 | 7.0 | 16493 | 0.1 |

**Table 1** List of 18 global mainshocks (above the horizontal double line) that generated stresses $\geq\sim$10 kPa with epicentral distance > 500 km from the study area (22°N, 70°S) and 11 M7+ mainshocks in Japan (below the horizontal double line) within 500 km of the Tohoku-Oki mainshock epicenter. Columns to the right of the origin information include the distance to the study area and the stress values based on theoretical PGV estimates (see Section 2.1).

tify and remove noisy data. The expectation is that if triggering occurs, the final stack will show an increase in the elevated measurements after time zero. We assess if elevated signals occur qualitatively by inspection, focusing on identifying obvious cases of increased rates after the teleseismic wave arrivals.

# 3 Results

We compute the statistical catalog tests and waveform analysis for our select 29 mainshocks: 18 of which are located at distances of 500 km or more from the study-area centroid and generate stress perturbations of ∼10 kPa or more, and the remaining 11 M7+ events are located within 500 km of the Tohoku Oki mainshock generate stress values of $\geq\sim$0.1 kPa, where comparable stress magnitudes have also generated triggered earthquakes in other regions (van der Elst and Brodsky, 2010; Peña Castro et al., 2019; Fan et al., 2021). We first present the results of the statistical analysis, followed by the waveform analysis, in Sections 3.1 and 3.2.

## 3.1 Statistical tests using the local earthquake catalog

The $P$-value calculations using the updated Sippl et al. (2023) local catalog show no statistically significant seismicity rate increases (i.e., $P \geq 95\%$) that were sustained over two or more time windows for any of the candidate global mainshocks or the Japan mainshocks (See Fig. S2). Velasco et al. (2008) found that stacking histogram data may enhance subtle triggering signals that may otherwise be obscured. However, in this work, we find that stacked histograms of seismicity bracketing all candidate mainshocks also show no evidence of any subtle triggering signal for the region that is visible considering the entire local catalog in aggregate (Fig. 2).

In contrast, all but one of the candidate mainshocks are associated with elevated gridded $P$-values on two or more nodes that demonstrate localized triggering (detailed below in Sec. 3.2). The spatial correlation of high values suggests a higher triggering propensity (higher triggerability) relative to other regions, which we can test using a comparison with the random data. We build three maps to demonstrate that the regions of high triggerability do not occur by chance: (1) the maximum $P$-

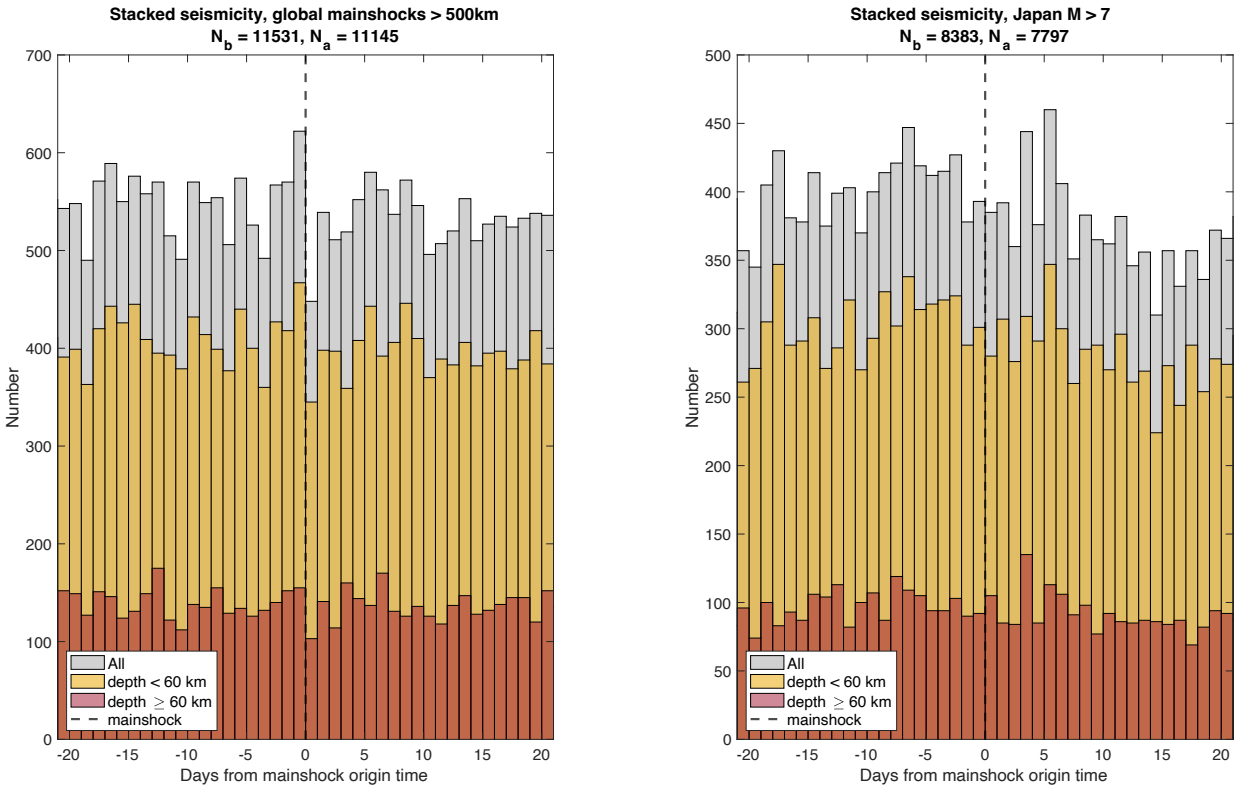


**Figure 2** Stacked histograms of local daily seismicity. Histograms show local catalog seismicity in 1-day bins bracketing the candidate mainshocks for (left) global events outside of the study area that generate stress values ≥10 kPa and (right) mainshocks in Japan with $M \geq 7$ that occurred within 500 km epicentral distance of the 2011 Tohoku-Oki megathrust rupture. Histograms are stacked for all candidate mainshocks in Tab. S1 (left) and Tab. S2 (right), with the total number of events for the before and after time periods shown above each panel. Individual histograms that go into stacks are shown in Fig. S2. Histograms are also divided into depth categories, similar to the division imposed by Sippl et al. (2023), where gray shows total cataloged events, yellow are events with depths <60 km, and red are events with depths ≥60 km.

values for all time windows averaged over all candidate global mainshocks; (2) as in (1) but for the Japan mainshocks; and (3) as in (1) and (2), but using the random time windows (Fig. 3). We then normalize the global and Japan maps by the random map (Sec. 3.1).

Both the global and Japanese mainshock candidates generate consistently high seismicity responses in common sub-regions (Fig. 3a and b). Notably, the area near Mejillones Peninsula in the southwest of the study area exhibits locally elevated $P$-values within a confined area (centered roughly on 23.5°S, 70.5°W, Fig. 3). Victor et al. (2018) document ubiquitous observations of observed triggered aseismic slip, including surface rupture observations in the same region. They also observed triggered aseismic slip on the Chomache Fault system (near 20°S, 70°W), where the catalog shows no evidence for elevated $P$-values. However, as we show below, the waveform analysis suggests that triggered activity may have occurred, but the catalog of completeness level (∼2.7) was too high for these likely small events to be cataloged. Both sets of mainshocks show a tendency for higher $P$-values in the southern central portion of the catalog footprint, which is also visible in the individual mainshock $P$-value grids (Figs. S3, S4). By comparison, the random origin times generate no notable spatially coherent patterns (Fig. 3c), suggesting that the signals in (a) and (b) result from triggering.

## 3.2 Waveform analysis

We next interrogate the three-component seismic waveforms to determine if triggering is occurring, but is not detectable using only catalog data. This is an important step, as the magnitude of completeness for the Sippl et al. (2023) catalog data is relatively high at 2.7 according to (Hainzl et al., 2019), and prior studies have found that remote triggering often involves smaller triggered events (M∼≤2) (Pankow and Kilb, 2020; Yao et al., 2021). An additional complication is that during upticks in seismicity rates, earthquake signals might overprint each other, making individual earthquakes difficult to decipher using automated methods (Kilb et al., 2007). Examining waveforms has the potential to provide additional information that might be missing from the catalog.

We apply the envelope method (Sec. 2) to the 18 M6.8+ candidate global mainshocks identified by the statistical tests, and the 11 Japan M7+ events (Tab. 1). In general, larger earthquakes are visible across the full network, whereas smaller events are only detectable at a handful

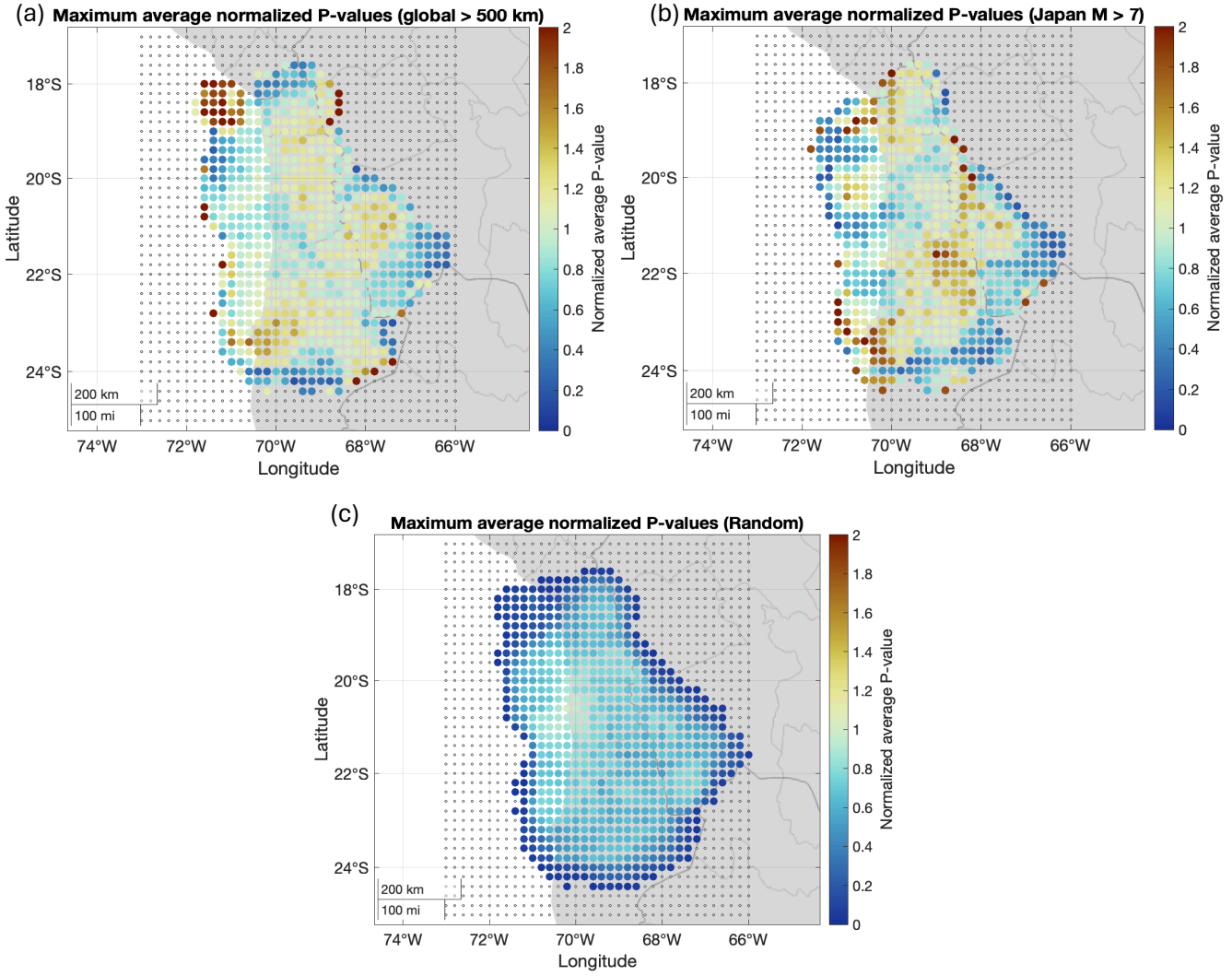


**Figure 3** Spatial investigation of $P$-value maps (normalized). $P$-value estimates quantifying the significance of seismicity rate changes averaged over all candidate mainshocks for ∼20 km radius circles centered on each grid node. The color-coded value is the maximum of the range of averaged estimates of all time windows ($t$ = ±1, 7, 10, 14 days), where cool colors indicate minimal rate changes and warm colors indicate larger rate changes. (a) Global mainshock results (> 500 km from the study area centroid), (b) Japanese $M>7$ mainshock results, and (c) random times simulating artificial mainshock results. (a) and (b) are normalized by the maximum artificial random value, and (c) is normalized by the maximum grid point value. Note: warm colors at the edges of grids are an artifact of normalizing by small numbers of earthquakes where seismic station coverage decreases.

of stations (Fig. 4 and 5). These waveforms reveal many smaller events missing from the Sippl et al. (2023) catalog (e.g., see Fig. 4, 5 and also see Fig. 6 events A, B, and E). Consistent with remote triggering that has already been identified for the 2011 M9.1 event (Victor et al., 2018), envelope stacks show high amplitudes during the time period of the teleseismic wave arrivals (Fig. 4a and c), and similar behavior is found for the 2024 M7.5 event (Fig. 5a and c).

For the 2011 M9.1 Japan mainshock waveform data, we find at least 10 earthquake signals that are not associated with a local catalog event, indicating these events are missing from the catalog (Fig. 4). Similarly, results from the 2024 M7.5 Japan event, which occurred after the time range of the local catalog, show at least five smaller events (similar in amplitude to the 2011 missed events), suggesting again that small-magnitude earthquakes are prevalent within these time windows and are likely too small to be included in local catalogs (Fig. 5b). Notably, for the 2024 waveform data, there appears to be an uptick in seismicity starting right after the larger-amplitude surface waves, where the largest local earthquake signal is within the coda of the teleseismic energy (Fig. 5a and c).

Indeed the envelope results show elevated signals following the teleseismic wave arrivals, but are these signals from local earthquakes? We could carefully analyze the waveforms, identify P- and S-waves, and augment the Sippl et al. (2023) catalog with newly discovered events. Although useful, that effort would be time-consuming and beyond the scope of this work. Instead, we examine in detail data from the 2008-07-19 M4 earthquake, which occurred north of our study region, to ensure the seismic wave arrival move-out signatures are

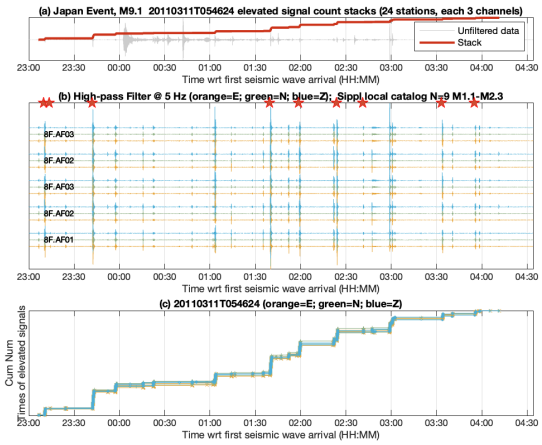


**Figure 4** Envelope results for the Japan 2011 M9.1 earthquake data: (a) Stack of all envelopes juxtaposed on an unfiltered waveform that shows the telesismic signals arrivals. (b) Filtered (5 Hz high pass) data from stations that have three components of data (color-coded). Red stars denote Sippl et al. (2023) catalog event times. As expected, the larger local events are recorded across the full network, and smaller local events are only visible on a handful of stations. There is evidence of additional smaller earthquakes not in the Sippl catalog (vertical bands of higher energy not associated with red stars). (c) Cumulative envelope stacks from each station (restricted to stations that have three components of data available).

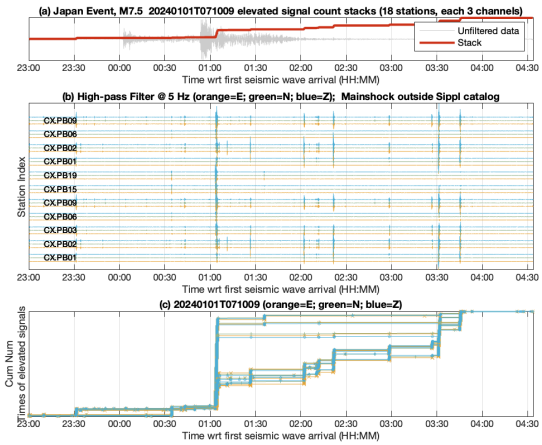


**Figure 5** Envelope results for the Japan 2024 M7.5 earthquake data, as in Fig. 4. The Sippl et al. (2023) catalog only spans 2007-2021, so no local catalog data is available for this 2024 Japan earthquake (i.e., no red stars as in Fig. 4 as this mainshock occurred after the end of the Sippl et al. (2023) catalog). Note the uptick in the number of elevated signals following the larger amplitude surface waves at ∼1 hour after the teleseismic waves arrived, which align with the larger amplitude teleseismic waves.

consistent with local earthquakes (Fig. 6). For each of these three-component data (11 stations), we identify P- and S-wave arrival times. These arrivals are impulsive, high-frequency bursts of energy, a signature typical for local earthquakes. A linear fit to the source-station distance vs. seismic wave arrival time data is used to compute seismic wave speeds. We find minimal variation from the linear fit line, suggesting these estimated speeds are robust. The estimated speeds are 8.2 and 4.8 km/s for P-wave and S-wave energy, respectively. These speeds are consistent with those reported by Kaila et al. (1999) for this region. Kaila et al. (1999) reported that the P-wave velocity ranged from 8.04 km/s at 40 km to 8.28 km/s at 250 km depth and that the S-wave velocity remained almost constant at 4.62 km/s at 40 to 210 km depth. We, therefore, conclude that these elevated signals are from a local earthquake, which corroborates the statistical analysis (Fig. 6). We leave a detailed enhancement of the local catalog at targeted regions, suggestive of elevated triggering potential, for future work.

## 4 Discussion

Returning to our original premise that large stresses play a role in remote aftershock triggering, we leverage the findings of Victor et al. (2018) that observed aseismic slip triggering in the Atacama Fault system of the Chilean subduction forearc by stresses on the order of ∼1 kPa. Both sets of mainshocks, namely, the 18 global events and 11 Japanese earthquakes (Tab. 1), fail to generate broad, statistically significant seismicity-rate changes when considering the catalog as a whole (Fig. 2). However, all candidate global mainshocks that occurred during the time period overlapping with the local catalog generated significant $P$-values ($\geq 0.95$) at two or more grid points (Fig. 3, Fig. S3).

Fan et al. (2021) and references therein note that the $\beta$-statistical test (also a difference-of-means test) alone may not be sufficient to establish the presence or absence of broad triggering behavior due to spatial and temporal differences in the $\beta$-parameter. In our initial efforts, we also wanted to include the study of near-field triggering from local mainshocks, which would require declustering the local catalog to differentiate clustered and background seismicity (Zaliapin and Ben-Zion, 2020). These initial declustering efforts suggested that, qualitatively, Chile appears to host comparatively large temporal (and potentially spatial) fluctuations in background seismicity relative to what has been found in other tectonic settings. Specifically, using a nearest-neighbor declustering method, we found background and clustered earthquakes in northern Chile difficult to separate. Indeed, the vast depth extent and spatially heterogeneous magnitude of completeness level of the local catalog made declustering challenging, making near-field triggering efforts intractable using the currently available data. Our initial declustering efforts revealed that a near-field triggering study in a complex region such as northern Chile would be challenging. It also remains unclear whether a near-field study would provide any additional insights into the heterogeneous triggering behavior already observed with the far-field data that would point unambiguously to causative mechanisms. We therefore leave our focus exclusively on remote triggering.

The large variations in background earthquake rates

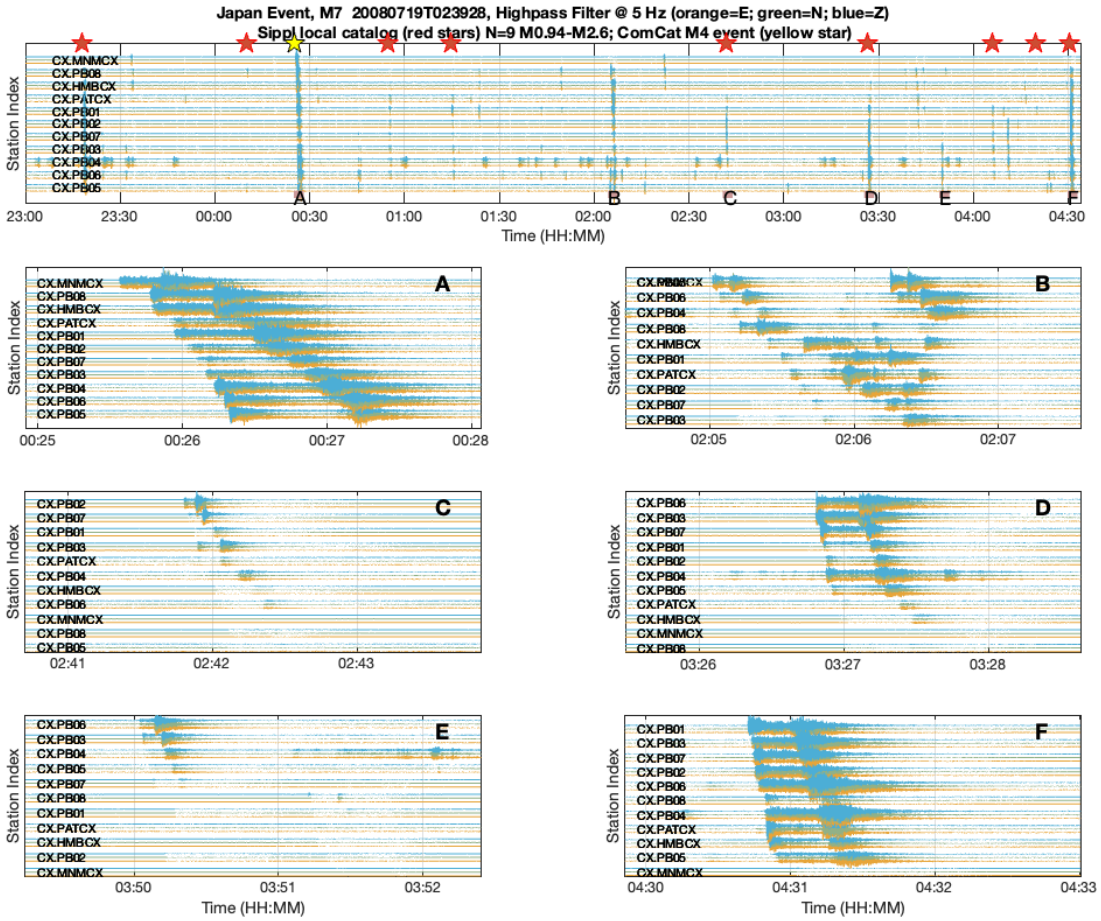


**Figure 6** (Top) Filtered waveforms (5 Hz high-pass) from CX network stations that recorded the 2008-07-19, M7, Japan, earthquake (depth 22 km). To confirm whether the elevated signals are indeed local earthquakes, select times of elevated signals are selected (Labeled A, B, C, D, E, and F). Origin times of local earthquakes in the Sippl et al. (2023) catalog are shown with red stars, and an M4 earthquake from the ComCat catalog is shown with a yellow star. The M4 earthquake is not in the Sippl catalog. Lower six plots: detailed examination of labeled waveforms from the top plot. These waveforms exhibit the signature of local earthquakes with visible P- and S-wave phases and variable start times indicative of local or regional earthquakes. Events B and E are not in the Sippl catalog but are clearly earthquakes. Event B is likely missing because it contains multiple earthquakes that overprint each other, and Event E is likely below the completeness level of the catalog. Based on the ComCat catalog, Event A is an M4 earthquake located in the northern part of the study region, farther away from the stations, as confirmed by the larger differences in arrival times. It is unclear why this M4 earthquake is missing from the Sippl catalog.

in northern Chile might lead to variations in linear threshold behavior where triggered earthquakes occur after a given strain or stress threshold is surpassed, similar to what is suggested in Fan et al. (2021). If triggering behavior is more closely aligned with other factors, such as receiver-fault orientation, faulting style, or temporally-dependent strength conditions, then a higher-resolution picture as afforded by the more spatially detailed $P$-value grids might lend more insight to spatially variations in triggerability. Several recent studies that employ dense data sets document local-scale variability in triggering behavior, which suggests it is more the rule than the exception (e.g., Peña Castro et al., 2019; Johnson et al., 2020; Pankow and Kilb, 2020; Fan et al., 2021; DeSalvio and Fan, 2023). The results presented here are consistent with these findings, showing local scale differences in remote triggering capabilities.

## 4.1 Remote triggering's relationship to the geological setting

Considering statistical catalog tests on the smaller spatial scale of ∼20 km demonstrates that patterns of triggerability do emerge. The gridded $P$-value tests show areas of consistently higher triggerability for both the global and Japanese candidate mainshocks in three primary regions. These include the onshore area near the Mejillones peninsula that lies between 23-24°S and 69-71°W, the area between 18.5-21°S and 69-70.5°W, and the 21-23°S and 67-69°W (Fig. 3). The Mejillones peninsula, which has hosted aseismic slip triggering (Victor et al., 2018), has been interpreted as a location of low

locking that potentially serves as a rupture barrier to megathrust earthquakes (Mètois et al., 2013; González et al., 2021). Victor et al. (2011) demonstrated that this rupture barrier is a persistent feature, at least on Quaternary time scales. From the integration of seismological and geological observations and quantification of the slip deficit beneath the Peninsula, they suggest that below it, a velocity strengthening barrier also exists. They hypothesize that the barrier will cause stress to be released aseismically via afterslip on the interface with accompanying upper plate deformation expressed in augmented upper plate fault activity at the same latitude. The augmented density of active upper plate faults in this area again may contribute to the locally higher triggering susceptibility.

The second patch of higher triggerability between the latitudes 18.5°S and 21°W can potentially be explained by a slowly decaying stress perturbation at depth, or by stress transferred to the upper plate after the 2005, M7.8 Tarapaca earthquake that occurred at a depth of 116 km. Peyrat et al. (2006) suggested that this earthquake was a slab pull event, reactivating an inherited fault due to dehydration embrittlement. This embrittlement process is caused by major faults in the downgoing oceanic plate stimulating hydrous alterations at depth in the Wadati-Benioff Zone, which could supply fluids for redistribution as a triggering mechanism (Peacock, 2001).

As for the third area of higher triggerability, namely, the latter, easternmost area, the 3D-seismicity distribution suggests that the patch may be associated with the band of seismicity at 80+ km depth along the plate interface that has been associated with slab de-watering (Dobson et al., 2002; Hyndman and Peacock, 2003; Rüpke et al., 2004). However, the spatial distribution of earthquakes that occur following the mainshock stressing events is also distributed along shallow faults in the forearc (Figure S4). Thus, the seismicity response to stress transients is not confined to the upper plate or the plate interface alone (Figs. S2, S4). Here, we do not try to distinguish plate interface with intraplate events in the down-going slab, but focus on the interaction between the subduction system and the forearc faults. Notably, all three areas with heightened triggerability are located near faults or fault patches that host a potential range of slip speeds and frictional behavior. In other words, a propensity for triggering may be related to localized changes in fault frictional behavior. The 3D distribution of earthquakes that respond to stress changes within northern Chile suggests that localized changes in frictional behavior may occur within forearc faults in the overriding plate as well as within the plate interface fault system (Fig. S4).

## 4.2 Possible antipodal triggering

It has been conjectured for decades that seismic waves might be amplified at the mainshock's antipode (location on the opposite side of the earth) because at this location, theoretically, seismic waves constructively add together (Butler and Tsuboi, 2010; Guglielmi, 2015). This focusing phenomenon could be operational at distances within 30° of the antipode (O'Malley et al., 2018). Other studies rebut this hypothesis, claiming that random chance can not be ruled out (Sullivan, 2012). More detailed studies indicate that although focusing can be observed in P-wave phases such as PKP or PP, heterogeneity in the travel paths can mask the focusing of S-wave phases, reducing the amplifications substantially (Retailleau et al., 2014). In this work, the 11 Japanese earthquakes are primarily within the allowable 30° range, spanning ranges 28°-35°. Thus, we can explore if antipodal triggering might be taking place, even though the stresses imparted by these Japan mainshocks are on the small end of what has been observed to generate triggered earthquakes (Fig. 7). As noted above, 10 of 11 of the Japanese events show evidence of local pockets of remote triggering (Fig. S4), and the waveform analysis reveals an increase in local earthquake activity that is primarily missing from the local catalog. Both of these observations are consistent with the idea that antipodal triggering might be occurring on a very localized level. But, the question of the effect of focusing remains open, as it is impossible to rule out that the perturbations alone were sufficient to generate these localized responses (Fig. S4).

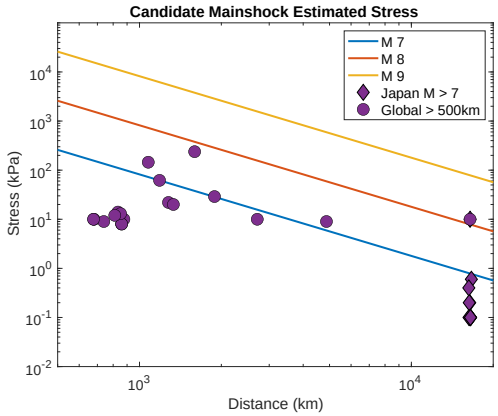


**Figure 7** Dynamic-stress generated by 29 candidate mainshocks (Fig. 1a) calculated using Eqs. 1 - 3 and the reported magnitudes. Symbols correspond to the shapes in Fig. 1, where circles correspond to global mainshocks with epicentral distances that exceed 500 km from the study centroid and that generated stress values of $\geq\sim$10 kPa. Diamonds correspond to M7+ events with epicentral distances within 500 km of the 2011 Tohoku-Oki mainshock, which triggered observed aseismic slip within the study region (Victor et al., 2018). Lines show the expected dynamic-stress decay with distance for mainshocks of magnitude 7, 8, and 9 for reference. Note that both axes are logarithmic in scale.

## 4.3 Possible triggering mechanisms

Our results show that triggerability in northern Chile is localized and does not follow any obvious stress triggering threshold behavior. The catalog statistical and waveform analyses demonstrate that triggering occurs on both instantaneous and delayed time scales of up to

14 days (the maximum time window tested, seen for one global mainshock and one mainshock in Japan, Fig. S2). The range of stress values that generate local seismicity changes appears to be highly variable, where triggering stresses for global mainshocks range between 8 - 300 kPa and Japanese mainshocks between 0.1 - 10 kPa. This wide span in stress that encompasses over two-orders of magnitude is inconsistent with a single stress-triggering threshold. However, these triggering-stress magnitudes are comparable to magnitudes that have generated triggering in a number of other regions, including regions of both intrinsically high and low natural seismicity rates (e.g., Brodsky and van der Elst, 2014; Wang et al., 2015; Peña Castro et al., 2019; Fan et al., 2021; Saini et al., 2023). The lack of an obvious stress threshold over which triggering consistently occurs (i.e. pushes receiver faults over their strength threshold) and the variability in the timing of the response, render linear mechanisms insufficient to explain these observations. So, for example, Coulomb failure (alone) can not tell the full story, suggesting that triggering is a more complex process involving multiple factors.

Linear triggering threshold behavior may be at play in localized areas. However, the range of stress values (10 kPa - 0.1 MPa) inferred from estimated PGV and the small-scale, localized response make a detailed investigation of a single threshold unattainable. To correctly study remote triggering requires an earthquake catalog with a consistently low magnitude of completeness level and an associated waveform dataset. The variability in the triggering response we found in this work provides evidence that non-linear triggering mechanisms may also be at work in northern Chile. For example, fluid redistribution as a response to dynamic-stress forcing commonly occurs in a subduction environment (e.g., Nakajima and Uchida, 2018; Gosselin et al., 2020), where the response of porous saturated media may cause triggering responses on both immediate and extended time scales resulting from redistribution of fluid pressure (e.g., Brodsky et al., 2003; Candela et al., 2015; Jin et al., 2021). Delayed triggering of up to 14 days may also be a result of variable fault frictional behavior, as has been observed for tremor and low-frequency earthquakes that occur in regions where fault frictional properties transition from slip-weakening to slip-strengthening (Rubenstein et al., 2007; Shelly et al., 2011; Dong et al., 2022). Elevated triggering susceptibility has been observed in faults that are near or bordering patches where aseismic slip occurs, i.e. at the boundary of seismogenic areas (Luo and Wiens, 2020; Fan et al., 2021). Specifically, Fan et al. (2021) observed triggering where frictional properties change along strike, similar to the assumed changes that occur at the 80-100 km depth band along dip in northern Chile at the slab de-watering limit.

If stressing events from mainshocks also trigger aseismic slip, which has already been documented in the forearc (Victor et al., 2018), then the triggered aseismic slip might generate secondary triggering of seismic events as a cascading response, as has been observed in more controlled environments related to induced earthquakes (e.g., Yu et al., 2021; Eyre et al., 2022). It has been proposed that dynamic-stressing can also change the distribution of frictional contacts in granular fault media or asperity contacts, which can lead to both an immediate and delayed triggering response (Ferdowsi et al., 2015; Dong et al., 2022). Notably, the areas of high triggering propensity, as indicated by the small-scale $P$-value patterns, are spatially correlated with regions of lower locking inferred from models based on GNSS data inversion (Fig. 3; Mètois et al. (2013)). The spatial correlation of triggering propensity and regions of low locking is consistent with critically stressed faults nucleating slip with an extra "push", and or secondary triggering resulting from aseismic-slip triggering, as well as a change in the critical slip distance.

A caveat that needs to be considered for this study is that the Sippl et al. (2023) catalog has a completeness level of 2.7, which means it lacks many of the small-magnitude earthquakes ($M<2$) that are often required to identify remote triggering (e.g., Prejean and Hill, 2018), and references therein). Along this same line, Pankow and Kilb (2020) found a lack of triggering in the ANZA region using a catalog that had a variable level of completeness. In 1985-1991, the level was $\sim$2, which, as expected, diminished with time, eventually falling to 0.8 in 2003 and beyond. A lack of triggering was also found by Kane et al. (2007) in an earlier work that also used a catalog with a completeness level of $\sim$1.5. More recent work, however, suggests that triggering in the ANZA region is ubiquitous (DeSalvio and Fan, 2023). This finding of ubiquitous triggering was reached using the Quake Template Matching catalog (Ross et al., 2019), which has a much lower completeness level ($\sim$-0.5 for select grid points). The contrasting interpretations regarding triggerability suggest that small magnitude earthquakes, perhaps magnitudes below $\sim$1.0, and detailed information regarding receiver faults and waveform signatures are key in identifying remote triggering. Thus, future studies aimed at identifying the multiple possible linear and non-linear mechanisms that generate triggered earthquakes in northern Chile will need to employ a detailed analysis in a region with dense station coverage and knowledge of geological structures. This study makes an important initial step of establishing that heterogeneous triggering occurs in northern Chile, and provides evidence that geological conditions play a role in controlling triggerability. It also shows that such a focused, localized study may be fruitful in the three targeted areas of northern Chile where localized triggering has been identified.

## 5 Conclusions

In this work, we search for remote triggering from mainshocks located 500 km or more from our study area's centroid. Out of an initial mainshock catalog of 11,878 events that occurred during the time span of our local earthquake catalog (1 January 2007 - 31 December 2021), 18 mainshocks produce local peak dynamic-stresses $\geq$8 kPa that generated local, statistically-significant seismicity-rate changes consistent with higher triggering potential. In addition, 10 out of the 11 M7+ events from the Japan region located

near the Tohoku Oki mainshock generated local seismicity rate increases on time scales ranging from hours to 14 days. The one exception was the 13 February 2021, M7.1 mainshock, which generated one of the smallest stress values (0.1 kPa). Considering the full study area as a continuum, we don't find any widespread triggering, as found in other regions (Pankow et al., 2004). However, we do find spatial pockets where triggering is more prevalent on a more granular level with length scale ∼20 km. Overall, remote triggering in northern Chile does not statistically exhibit any obvious threshold behavior in which large stress perturbations consistently generate a pronounced triggering response. Waveform data from CX, 8G, and 8F network stations enable identification of elevated seismic waveform signals indicative of local seismicity using 5 Hz high-pass filtered waveforms from 3-component broadband data. The elevated local seismic energy at representative stations suggests there were additional triggered earthquakes missing from the local catalog. Our statistical tests and waveform results are consistent with antipodal triggering but are not robust enough to rule out other triggering factors.

Our results show evidence for localized, elevated triggerability both near the subduction interface and on shallow faults in the forearc in Northern Chile during the time period from 2007 through 2021. Notably, local areas with heightened triggering capability may be spatially correlated with regions of low frictional locking, which is consistent with previous observations of remote, dynamic aseismic slip triggering. The correlation of heightened triggering propensity to low-locking, the lack of a stress triggering threshold, and the range of response times are consistent with non-linear triggering mechanisms, such as material fatigue, aseismic-slip triggering, and fluid-pressure redistribution within the subduction fault system. In summary, both catalog and waveform analysis provide evidence for localized pockets of triggering in Northern Chile, although there is an absence of broad seismicity rate changes across the larger study region. The findings of this study suggest that a detailed study of triggering in northern Chile at the three sites where aseismic slip has been documented may be warranted to further elucidate the causative mechanisms that nucleate slip on receiver faults with stresses on the order of ∼0.1 - 10s of kPa.

## Acknowledgements

The authors would like to thank Alice Gabriel and Wenyuan Fan for helpful discussions that improved the quality of this manuscript. RH was supported by the Volkswagen Stiftung. DK was supported by start-up package funds. We would also like to thank associate editor A. Llenos, as well as B. Enescu and one anonymous reviewer for their helpful comments.

## Data and code availability

All data and code used to conduct this study are publicly available. Global earthquake catalog data are from the ANSS Comprehensive Earthquake Catalog curated by the U. S. Geological Survey, and can be found under the following link: https://earthquake.usgs.gov/data/comcat/. Local earthquake data are from the Sippl et al. (2023) catalog, and waveform data are archived and downloadable from the following websites: GFZ Seismological Data Archive: https://geofon.gfz-potsdam.de/waveform/archive/; Seismological Facility for the Advancement of Geoscience (SAGE): https://ds.iris.edu/ds/nodes/dmc/data/types/waveform-data/. The code used for analysis and visualization was programmed in MATLAB version: 9.13.0 (R2022b), The MathWorks Inc. (2022); the scripts used to calculate statistical significance are available under the following link: https://www.dropbox.com/scl/fi/yg0jdtr1kain63pa57no6/HarringtonetalCodes.zip?rlkey=n5fbs64ibh87hlw3g1zzxeawo&dl=0. We would like to thank Nicolas van der Elst for his advice in calculating P-values in MATLAB.

## Competing interests

The authors have no competing interests.

## References

Aiken, C. and Peng, Z. Dynamic triggering of microearthquakes in three geothermal/volcanic regions of California. *J. Geophys. Res.*, 119:6992 – 7009, 2014. doi: 10.1002/2014JB011218.

Aki, K. and Richards, P. G. *Quantitative seismology*. 2002.

Alfaro-Diaz, R., Velasco, A. A., Pankow, K. L., and Kilb, D. Optimally oriented remote triggering in the Coso geothermal region. *Journal of Geophysical Research: Solid Earth*, 125(8): e2019JB019131, 2020. doi: 10.1029/2019JB019131.

Bansal, A. R. and Ghods, A. Remote triggering in Iran: large peak dynamic stress is not the main driver of triggering. *Geophys. J. Int.*, 225(1):456–476, 2021. doi: https://doi.org/10.1093/gji/ggaa573.

Brodsky, E. E. and Prejean, S. G. New constraints on mechanisms of remotely triggered seismicity at Long Valley Caldera. *J. Geophys. Res.*, 110(B04302), 2005. doi: 10.1029/2004JB003211.

Brodsky, E. E. and van der Elst, N. J. The Uses of Dynamic Earthquake Triggering. *Ann. Rev. of Earth and Planet. Sci.*, 42(1): 317–339, 2014. doi: 10.1146/annurev-earth-060313-054648.

Brodsky, E. E., Roeloffs, E., Woodcock, D., Gall, I., and Manga, M. A mechanism for sustained groundwater pressure changes induced by distant earthquakes. *J. Geophys. Res.*, 108(B8), 2003. doi: 10.1029/2002JB002321.

Butler, R. and Tsuboi, S. Antipodal seismic observations of temporal and global variation at Earth's inner-outer core boundary. *Geophys. Res. Lett.*, 37(11), 2010. doi: 10.1029/2010GL042908.

Candela, T., Brodsky, E. E., Marone, C., and Elsworth, D. Flow rate dictates permeability enhancement during fluid pressure oscillations in laboratory experiments. *J. Geophys. Res.*, 120: 2037–2055, 2015. doi: 10.1002/ 2014JB011511.

DeSalvio, N. D. and Fan, W. Ubiquitous earthquake dynamic triggering in Southern California. *Journal of Geophysical Research: Solid Earth*, 128(6):e2023JB026487, 2023. doi: 0.1029/2023JB026487.

Dixit, M., Bansal, A. R., Kumar, M. R., Kumar, S., and Teotia, S. S. The sensitivity of the intraplate Kachchh Rift Basin, NW India to the direction of incoming seismic waves of teleseismic earth-

quakes. *Geophys. J. Int.*, 232(1):17–36, 2023. doi: https://-doi.org/10.1093/gji/ggac289.

Dobson, D. P., Meredith, P. G., and Boon, S. A. Simulation of subduction zone seismicity by dehydration of serpentine. *Science*, 298:1407–1410, 2002. doi: 10.1126/science.1075390.

Dong, P., Chen, K., Xia, W., Yao, Z., Peng, Z., and Elsworth, D. Earthquake Delay and Rupture Velocity in Near-Field Dynamic Triggering Dictated by Stress-Controlled Nucleation. *Seismol. Res. Lett.*, 94:913–924, 2022. doi: 10.1785/0220220264.

Enescu, B., Shimojo, K., Opris, A., and Yagi, Y. Remote triggering of seismicity at Japanese volcanoes following the 2016 M7.3 Kumamoto earthquake. *Earth, Planets and Space*, 68(165), 2016. doi: 10.1186/s40623-016-0539-5.

Eyre, T. S., Samsonov, S., Feng, W., Kao, H., and Eaton, D. W. InSAR data reveal that the largest hydraulic fracturing-induced earthquake in Canada, to date, is a slow-slip event. *Sci. Rep.*, 12 (2043):579–582, 2022. doi: 10.1038/s41598-022-06129-3.

Fan, W., Barbour, A. J., Cochran, E. S., and Lin, G. Characteristics of frequent dynamic triggering of microearthquakes in Southern California. *J. Geophys. Res.*, 126(e2020JB02082), 2021. doi: 10.1029/2020JB020820.

Ferdowsi, B., Griffa, M., Guyer, R. A., Johnson, P. A., Marone, C., and Carmeliet, J. Acousti- cally induced slip in sheared granular layers: Application to dynamic earthquake triggering. *Geophys. Res. Lett.*, 42:9750–9757, 2015. doi: 10.1002/2015GL066096.

Freed, A. M. Earthquake triggering by static, dynamic, and postseismic stress transfer. *Annu. Rev. Earth Planet. Sci.*, 33:335–367, 2005. doi: 10.1146/annurev.earth.33.092203.122505.

Gomberg, J., Reasenberg, P., Bodin, P., and Harris, R. A. Earthquake triggering by seismic waves following the Landers and Hector Mine earthquakes. *Tectonophysics*, 745:462–466, 2001. doi: 10.1038/35078053.

Gomberg, J., Bodin, P., Larson, K., and Drager, H. Earthquake nucleation by transient deformations caused by the M = 7.9 Denali, Alaska, earthquake. *Nature*, 427:621–624, 2004. doi: 10.1038/nature02335.

Gombert, B. and Hawthorne, J. C. Rapid tremor migration during few minute-long slow earthquakes in Cascadia. *J. Geophys. Res.*, 128(e2022JB025034):115–125, 2023. doi: 10.1029/2022JB025034.

González, G., Pasten-Araya, P., Victor, P., González, Y., Valenzuela, J., and Shrivastava. The role of interplate locking on the seismic reactivation of upper plate faults on the subduction margin of northern Chile. *Sci. Reports*, 11, 2021. doi: 10.1038/s41598-021-00875-6.

Gosselin, J. M., Audet, P., Estève, McLellan, M., Mosher, S. G., and Scaeffer, A. J. Seismic evidence for megathrust fault-valve behavior during episodic tremor and slip. *Bull. Seismol. Soc. Am.*, 109(eaay5174):372–386, 2020. doi: 10.1126/sciadv.aay5174.

Guglielmi, A. The cumulative effect of convergent seismic waves. *Izvestiya, Physics of the Solid Earth*, 51:915–919, 2015. doi: 10.1134/S1069351315060038.

Guglielmi, Y., Cappa, F., Avouac, J.-P., Henry, P., and Elsworth, D. Seismicity triggered by fluid injection–induced aseismic slip. *Science*, 348(6240):1224–1226, 2015. doi: 10.1126/science.aab0476.

Hainzl, S., Sippl, C., and Schurr, B. Linear relationship between aftershock productivity and seismic coupling in the northern Chile subduction zone. *J. Geophys. Res.*, 124:8726–8738, 2019. doi: 10.1029/ 2019JB017764.

Hardebeck, J. L. and Harris, R. A. Earthquakes in the shadows: Why aftershocks occur at surprising locations. *The Seismic Record*, 2 (3):207–216, 2022. doi: 10.1785/0320220023.

Hernandez, S., Brodsky, E. E., and van der Elst, N. J. The magnitude distribution of dynamically triggered earthquakes. *Geochem. Geophys. Geosyst.*, 15, 2014. doi: 0.1002/ 2014GC005404.

Hill, D. P. On the sensitivity of transtensional versus transpressional tectonic regimes to remote dynamic triggering by Coulomb failure. *Bull. Seismol. Soc. Am.*, 105(3), 2015. doi: 10.1785/0120140292.

Hill, D. P., Reasenberg, P. A., Michael, A., Arabaz, W. J., Beroza, G., Brumbaugh, D., Brune, J. N., Castro, R., Davis, S., dePolo, D., Ellsworth, W. L., Gomberg, J., Harmsen, S., House, L., Jackson, S. M., Johnston, M. J. S., Jones, L., Keller, R., Malone, S., Munguia, L., Nava, S., Pechmann, J. C., Sanford, A., Simpson, R. W., Smith, R. B., Stark, M., Stickney, M., Vidal, A., Walter, S., Wong, V., and Zollweg, J. Seismicity remotely triggered by the Magnitude 7.3 Landers, California, earthquake. *Science*, 260: 1617 – 1623, 1993. doi: 10.1126/science.260.5114.1617.

Husen, S., Wismer, S., and Smith, R. R. Remotely triggered seismicity in the Yellowstone National Park Region by the 2002 J = 7.9 Denali, Alaska earthquake. *Bull. Seismol. Soc. Am.*, 94: S317–S331, 2004. doi: 0.1785/0120040617.

Hyndman, R. D. and Peacock, S. Serpentinization of the forearc mantle. *Earth Planet. Sci. Lett.*, 212(3-4):417–432, 2003. doi: 10.1016/S0012-821X(03)00263-2.

Jin, Y., Dyaur, N., and Zheng, Y. Laboratory evidence of transient pressure surge in a fluid-filled fracture as a potential driver of remote dynamic earthquake triggering. *The Seismic Record*, 1 (2):66–74, 2021. doi: 10.1785/0320210015.

Johnson, C. W., Bürgmann, R., and Pollitz, F. F. Rare dynamic triggering of remote M $\geq$ 5.5 earthquakes from global catalog analysis. *Journal of Geophysical Research: Solid Earth*, 120(3): 1748–1761, 2015. doi: 10.1002/2014JB011788.

Johnson, C. W., Kilb, D., Baltay, A., and Vernon, F. Peak ground velocity spatial variability revealed by dense seismic array in southern California. *Journal of Geophysical Research: Solid Earth*, 125(6):e2019JB019157, 2020. doi: 10.1029/2019JB019157.

Johnson, P. A., Carmeliet, J., M., S. H., Scuderi, M., Carpenter, B. M., Guyer, R. A., Daub, E. G., and Marone, C. Dynamically triggered slip leading to sustained fault gouge weakening under laboratory shear conditions. *Geophys. Res. Lett.*, 43:1559–1565, 2016. doi: 10.1002/2015GL067056.

Kaila, K., Krishna, V., and Khandekar, G. Preliminary models of upper mantle P and S wave velocity structure in the western South America region. *Journal of Geodynamics*, 27(4-5):567–583, 1999. doi: 10.1016/S0264-3707(98)00016-7.

Kane, D. L., Kilb, D., Berg, A. S., and Martynov, V. G. Quantifying the remote triggering capabilities of large earthquakes using data from the ANZA Seismic Network catalog (southern California). *Journal of Geophysical Research: Solid Earth*, 112(B11), 2007. doi: 10.1029/2006JB004714.

Kilb, D., Gomberg, J., and Bodin, P. Triggering of earthquake aftershocks by dynamic stresses. *Nature*, 408(6812):570–574, 2000. doi: 10.1038/35046046.

Kilb, D., Martynov, V. G., and Vernon, F. L. Aftershock detection thresholds as a function of time: Results from the ANZA seismic network following the 31 October 2001 ML 5.1 Anza, California, earthquake. *Bulletin of the Seismological Society of America*, 97 (3):780–792, 2007. doi: 10.1785/0120060116.

King, G. C., Stein, R. S., and Lin, J. Static stress changes and the triggering of earthquakes. *Bulletin of the Seismological Society of America*, 84(3):935–953, 1994. doi: 10.1785/BSSA0840030935.

Lay, T. and Wallace, T. *Modern Global Seismology*. ISSN. Elsevier Science, 1995. https://books.google.de/books?id=CSCuMPt5CTcC.

Li, C., Peng, Z., Yao, D., Meng, X., and Zhai, Q. Temporal changes of seismicity in Salton Sea Geothermal Field due to distant earthquakes and geothermal productions. *Geophysical Journal International*, 232(1):287–299, 2023. doi: 10.1093/gji/ggac324.

Luo, Y. and Wiens, D. A. High rates of deep earthquake dynamic triggering in the thermal halos of subducting slabs. *Geophysical Research Letters*, 47(8):e2019GL086125, 2020. doi: 10.1029/2019GL086125.

MATLAB version: 9.13.0 (R2022b), The MathWorks Inc. MATLAB version: 9.13.0 (R2022b). https://www.mathworks.com.

Meng, X. and Peng, Z. Seismicity rate changes in the Salton Sea Geothermal Field and the San Jacinto Fault Zone after the 2010 Mw 7.2 El Mayor-Cucapah earthquake. *Geophys. J. Int.*, 197(3), 2014. doi: 10.1029/2004JB003277.

Mètois, M., Socquet, A., Vigny, C. Carrizon, D., Peyrat, S., Delorme, A., Maureira, E., Valderas-Bermejo, M.-C., and Orteg, I. Revisiting the North Chile seismic gap segmentation using GPS-derived interseismic coupling. *Geophys. J. Int.*, 194:1283–1294, 2013. doi: 10.1093/gji/ggt183.

Miyazawa, M. Propagation of an earthquake triggering front from the 2011 Tohoku-Oki earthquake. *Geophys. Res. Lett.*, 38 (L23307), 2011. doi: 10.1029/2011GL049795.

Nakajima, J. and Uchida, N. Repeated drainage from megathrusts during episodic slow slip. *Nature Geoscience*, 11(5):351–356, 2018. doi: 10.1038/s41561-018-0090-z.

Ogata, Y. Seismicity analysis through point-process modeling: A review. *Pure and App. Geophys.*, 155(2):471–507, 1999. doi: 10.1007/s000240050275.

Opris, A., Enescu, B., Yagi, Y., and Zhuang, J. Triggering and decay characteristics of dynamically activated seismicity in Southwest Japan. *Geophys. J. Int.*, 212(2):1010–1021, 2018. doi: 10.1093/gji/ggx456.

O'Malley, R. T., Mondal, D., Goldfinger, C., and Behrenfeld, M. J. Evidence of systematic triggering at teleseismic distances following large earthquakes. *Scientific reports*, 8(1):11611, 2018. doi: 10.1038/s41598-018-30019-2.

Pankow, K. L. and Kilb, D. Going beyond rate changes as the sole indicator for dynamic triggering of earthquakes. *Sci. Reports*, 10 (4120), 2020. doi: 10.1038/s41598-020-60988-2.

Pankow, K. L., Arabasz, W. J., Pechmann, J. C., and Nava, S. J. Triggered seismicity in Utah from the 3 November 2002 Denali fault earthquake. *Bulletin of the Seismological Society of America*, 94 (6B):S332–S347, 2004. doi: 10.1785/0120040609.

Peacock, S. Are the lower planes of double seismic zones caused by serpentine dehydration in subducting oceanic mantle? *Geology*, 29:299–302, 2001. doi: 10.1130/0091-7613(2001)029<0299:ATLPOD>2.0.CO;2.

Peña Castro, A., Dougherty, S. L., Harrington, R., and Cochran, E. S. Delayed dynamic triggering of disposal-induced earthquakes observed by a dense array in northern Oklahoma. *Journal of Geophysical Research: Solid Earth*, 124(4):3766–3781, 2019. doi: 10.1029/2018JB017150.

Peyrat, S., Campos, J., B., d. J., Perez, A., Bonvalot, S., Bouin, M.-P., Legrand, D., Nercessian, A., Charade, O., Patau, G., Clévédé, E., Kausel, E., Bernard, P., and Vilotte, J. P. Tarapacá intermediate-depth earthquake (Mw 7.7, 2005, northern Chile): A slab-pull event with horizontal fault plane constrained from seismological and geodetic observations. *Geophys. Res. Lett.*, 33(L22308), 2006. doi: 10.1029/2006GL027710.

Pollitz, F., Stein, R. S., Sevilgen, V., and Bürgmann, R. The 11 April 2012 east Indian Ocean earthquake triggered large aftershocks worldwide. *Nature*, 490(7419):250–253, 2012. doi: 10.1038/nature11504.

Prejean, S. G. and Hill, D. P. The influence of tectonic environment on dynamic earthquake triggering: A review and case study on Alaskan volcanoes. *Tectonophysics*, 745:293–304, 2018. doi: 10.1016/j.tecto.2018.08.007.

Prejean, S. G., Hill, D. P., Brodsky, E. E., Hough, S. E., Johnston, M. J. S., Malone, S. D., Oppenheimer, D. H., Pitt, A. M., and Richards-Dinger, K. B. Remotely triggered seismicity on the United States west coast following the M w 7.9 Denali fault earthquake. *Bull. Seismol. Soc. Am.*, 94(6B):S348–S359, 2004. doi: 10.1785/0120040610.

Prejean, S. G., Hill, D. P., and Myers, R. *Earthquakes dynamic triggering of*. Springer Heidelberg, 2010. doi: 10.1007/978-0-387-30440-3.

Reasenberg, P. Second-order moment of Central California seismicity, 1969-1982. *J. Geophys. Res.*, 90(B7):5479–5495, 1985. doi: 10.1029/JB090iB07p05479.

Retailleau, L., Shapiro, N., Guilbert, J., Campillo, M., and Roux, P. Antipodal focusing of seismic waves observed with the USArray. *Geophysical journal international*, 199(2):1030–1042, 2014. doi: 10.1093/gji/ggu309.

Ross, Z. E., Trugman, D. T., Hauksson, E., and Shearer, P. M. Searching for hidden earthquakes in Southern California. *Science*, 364 (6442):767–771, 2019. doi: 10.1126/science.aaw6888.

Rubenstein, J. L., Vidale, J. E., Gomberg, J., Bodin, P., Creager, K. C., and Malone, S. D. Non-volcanic tremor driven by large transient shear stresses. *Nature*, 448:579–582, 2007. doi: 10.1038/nature06017.

Rüpke, L. H., Morgan, J. P., Hort, M., and Connolly, J. Serpentine and the subduction zone water cycle. *Earth Planet. Sci. Lett.*, 223(1-2):17–34, 2004. doi: 10.1016/j.epsl.2004.04.018.

Saini, T., Bansal, A. R., Rao, N. P., Pasricha, R., and Vempati, V. Tiny stresses are capable of triggering earthquakes and tremors in Arunachal Himalaya. *Sci. Reports*, 13(22223), 2023. doi: https://doi.org/10.1038/s41598-023-49068-3.

Shelly, D., Peng, Z., Hill, D., and Aiken, C. Triggered creep as a possible mechanism for delayed dynamic triggering of tremor and earthquakes. *Nature Geosci.*, 4:384–388, 2011. doi: 10.1038/ngeo1141.

Sippl, C., Schurr, B., Asch, G., and Kummerow, J. Seismicity structure of the northern Chile forearc from> 100,000 double-difference relocated hypocenters. *Journal of Geophysical Research: Solid Earth*, 123(5):4063–4087, 2018. doi: 10.1002/2017JB015384.

Sippl, C., Schurr, B., Münchmeyer, J., Barrientos, S., and Oncken, O. The Northern Chile forearc constrained by 15 years of permanent seismic monitoring. *J. of S. Am. Earth Sci.*, 126(104326), 2023. doi: 10.1016/j.jsames.2023.104326.

Stein, R. S. The role of stress transfer in earthquake occurrence. *Nature*, 402:605 – 609, 1999. doi: 10.1038/45144.

Sullivan, B. Delayed triggering of early aftershocks by multiple surface waves circling the earth. Master's thesis, Georgia Institute of Technology, 2012.

Tape, C., West, M., Silwal, V., and Ruppert, N. Earthquake nucleation and triggering on an optimally oriented fault. *Earth Planet. Sci. Lett.*, 363:231–241, 2013. doi: 10.1016/j.epsl.2012.11.060.

U. S. Geological Survey. Earthquake Hazards Program, 2017, Advanced National Seismic System (ANSS) Comprehensive Catalog of Earthquake Events and Products. Technical report, U. S. Geological Survey, 2024. doi: 10.5066/F7MS3QZH.

van der Elst, N. J. and Brodsky, E. E. Connecting near-field and far-field earthquake triggering to dynamic strain. *J. Geophys. Res.*, 119(9):6992–7009, 2010. doi: 10.1029/2009JB006681.

Velasco, A. A., Hernandez, S., Parsons, T., and Pankow, K. Global

ubiquity of dynamic earthquake triggering. *Nature geoscience*, 1(6):375–379, 2008. doi: 10.1038/ngeo204.

Victor, P., Sobiesiak, M., Nielson, S., Glodny, J., and Oncken, O. Long-term persistence of subduction earthquake segment boundaries: Evidenc from Mejillones Peninsula, northern Chile. *J. Geophys. Res.*, 116(B02402), 2011. doi: 10.1029/2010JB007771.

Victor, P., Oncken, O., Sobiesiak, M., Kemter, M., Gonzalez, G., and Ziegenhagen, T. Dynamic triggering of shallow slip on forearc faults constrained by monitoring surface displacement with the IPOC Creepmeter Array. *Earth Planet. Sci. Lett.*, 502:57–73, 2018. doi: 10.1016/j.epsl.2018.08.046.

Wallace, L. M., Kaneko, Y., Hreinsdóttir, S., Hamling, I., Peng, Z., Bartlow, N., D'Anastasio, E., and Fry, B. Large-scale dynamic triggering of shallow slow slip enhanced by overlying sedimentary wedge. *Nature Geosci.*, 10:765–770, 2017. doi: 10.1038/ngeo3021.

Wang, B., Harrington, R. M., Liu, Y., Yu, H., Carey, A., and van der Elst, N. J. Isolated cases of remote dynamic triggering in Canada detected using cataloged earthquakes combined with a matched-filter approach. *Geophys. Res. Lett.*, 42, 2015. doi: 10.1002/2015GL064377.

Wang, B., Harrington, R. M., Liu, Y., Kao, H., and Yu, H. Remote dynamic triggering of earthquakes in three unconventional Canadian hydrocarbon regions based on a multiple-station matched-filter approach. *Bull. Seismol. Soc. Am.*, 109(1): 372–386, 2018. doi: 10.1785/0120180164.

Wang, B., Harrington, R. M., Liu, Y., Kao, H., and Yu, H. Remote dynamic triggering of earthquakes in three unconventional Canadian hydrocarbon regions based on a multiple-station matched-filter approach. *Bulletin of the Seismological Society of America*, 109(1):372–386, 2019. doi: 10.1785/0120180164.

Wei, S., Avouac, J.-P., Hudnut, K. W., Donnellan, A., Parker, J. W., Graves, R. W., Helmberger, D., Fielding, E., Liu, Z., Cappa, F., and Eneva, M. The 2012 Brawley swarm triggered by injection-induced aseismic slip. *Earth Planet. Sci. Lett.*, 415:115–125, 2015. doi: 10.1016/j.epsl.2015.03.054.

Yao, D., Peng, Z., Kaneko, Y., Fry, B., and Meng, X. Dynamic triggering of earthquakes in the North Island of New Zealand following the 2016 Mw 7.8 Kaikōura earthquake. *Earth and Planetary Science Letters*, 557:116723, 2021. doi: 10.1016/j.epsl.2020.116723.

Yu, H., Harrington, R. M., Kao, H., Liu, Y., and Wang, B. Fluid-injection-induced earthquakes characterized by hybrid-frequency waveforms manifest the transition from aseismic to seismic slip. *Nat. Comm.*, 12(6862), 2021. doi: 10.1038/s41467-021-26961-x.

Zaliapin, I. and Ben-Zion, Y. Earthquake declustering using the nearest-neighbor approach in space-time-magnitude domain. *J. Geophys. Res.*, 125(e2018JB017120), 2020. doi: 10.1029/2018JB017120.